Available online at www.sciencedirect.com
ScienceDirect
Ceramics International 36 (2010) 767–772
CERAMICS INTERNATIONAL
www.elsevier.com/locate/ceramint

Nanostructured alumina particles synthesized by the Spray Pyrolysis method: microstructural and morphological analyses

M.I. Martín [a,*], L.S. Gómez [a], O. Milosevic [b], M.E. Rabanal [a,**]

[a] University Carlos III de Madrid, Avda. de la Universidad, 30, 28911 Leganés, Madrid, Spain
[b] Institute of Technical Sciences of Serbian Academy of Sciences and Arts, K. Mihailova 35/IV, 11000 Belgrade, Serbia

Received 13 March 2009; received in revised form 20 September 2009; accepted 6 October 2009
Available online 3 November 2009

Abstract

Ultrafine particles or nanoparticles (ranging from a few nanometers to 100 nm) are of considerable interest for a wide variety of applications, ranking from catalyst to luminescence ceramics, due to their unique and improved properties primarily determined by size, composition and structure. This study presents the preparation and characterization of nanostructured spherical alumina particles by the Spray Pyrolysis method for the application in reinforcements of metal-matrix composites (MMCs). Synthesis procedure includes aerosol formation ultrasonically from alumina nitrate water solution and its decomposition into a tubular flow reactor at 700 °C. The obtained particles are spherical, smooth, amorphous and in non-agglomerated state. Microstructural and morphological analyses were carried out using X-ray diffraction (XRD), scanning electron microscopy (SEM/EDS) and analytical and high resolution transmission electron microscopy (TEM/HRTEM).

Keywords: Spray Pyrolysis; Alumina; Nanostructured Particles; Isothermal Treatment

1. Introduction

Nanometer-sized particles hold great potential for use in electronic, chemical or mechanical industries, as well as in relevant technologies, including superconductors, catalysts, magnetic materials, structural and engineering materials. Aluminium oxide nanoparticles have important applications in ceramic industry [1,2] and can be used as an abrasive material, in heterogeneous catalysis, as an absorbent, as a biomaterial and in reinforcements of metal-matrix composites (MMCs) [3–5]. Metal-matrix composites having fine-scale and uniformly dispersed phases, are of great technological interest because of improved mechanical properties, particularly the hardness, wear resistance, elastic modulus and yield strength [6,7]. The addition of ceramic alumina nanoparticles into MMCs might have significant industrial applications in the automotive and aerospace industries.

In order to be used for effective discontinuous reinforcements in a continuous metal-matrix, Al_2O_3 particles have to fulfill certain structural and morphological requirements: small particle size and narrow size distribution, large surface area, spherical morphology and the absence of agglomerates. As far as the hot wall aerosol synthesis method (Spray Pyrolysis), which is basically a chemical route for obtaining advanced materials, is concerned, it offers several advantages in the preparation of well-defined oxide powders over conventional synthesis [8].

The Spray Pyrolysis technique is based on ultrasonic generation of micrometric-sized aerosol droplets and their decomposition at intermediate temperatures (400–800 °C). Due to the fact that evaporation, precipitation, drying and decomposition occur in a dispersed phase and in a single step, it becomes possible to control important particle properties (size, morphology, chemical composition, etc.) simply by controlling the process parameters (residence time and decomposition temperature) [9–15]. The particles arise through the thermally induced processes of nuclei formation, collision and coalescence [9] after finalizing the processes of solvent evaporation/drying and consecutively solute precipitation and decomposition that occur at the droplet level.

* Corresponding author. Tel.: +34 913020440; fax: +34 913020700.
** Corresponding author. Tel.: +34 916249914; fax: +34 916249430.
E-mail addresses: MARIAIMH@hotmail.com (M.I. Martín), mariaeugenia.rabanal@uc3m.es (M.E. Rabanal).

0272-8842/$36.00.
doi:10.1016/j.ceramint.2009.10.013

Resulting spherical so called ''secondary particles'' then arise through the growth and aggregation of nanoscaled ''primary particles''. The secondary particle size and size distribution are mainly influenced by the properties of aerosol generator and precursor solutions. The primary particles, that represent either crystallites or block-mosaic assembles, could be coalesced entirely or densified.

This work describes the synthesis of nanostructured alumina particles by the Spray Pyrolysis method (at 700 °C) and the structural and morphological characterization of these nanoparticles for the application in metal-matrix composites for nanoreinforcements. The aerosol synthesis at 700 °C was chosen in order to synthesize the amorphous powder without the onset of crystallization and to promote and control the crystallization via additional thermal treatment.

2. Experimental procedure

2.1. Particle synthesis

The Spray Pyrolysis experimental set-up consists of an ultrasonic nebulizer (RBI), a quartz tube located inside a cylindrical furnace (LENTON, l–0.95 m) and a water collector (Fig. 1). An aqueous precursor solution was prepared by dissolving the corresponding amount of aluminium nitrate nonahydrate ($Al(NO_3)_3{\cdot}9H_2O$, p.a., 99.997% purity, Aldrich) in order to obtain 0.1×10^3 mol m^{-3} (0.0375×10^3 kg m^{-3}) concentration. The initial solution was atomized using an ultrasonic vibrating frequency of 2.1×10^6 s^{-1}. The aerosol was transported into a reaction zone and decomposed at 700 °C. Air was used as a carrier gas. Its flow rate was 2.5×10^{-5} m^3 s^{-1}, whereas the droplet/particle residence time, calculated from the carrier gas flow rate and the geometry of the reactor, was 18.6 s. The particles were water-collected at exhaust.

The mean droplet sizes of the generated aerosol droplets were estimated in accordance with the following Lang's equation [16]:

$$D_0 = 0.34\left(\frac{8\pi\gamma}{\rho f^2}\right)^{0.33} \quad (1)$$

where D_0 is the droplet mean size (μm), γ is the liquid (precursor solution) surface tension (10^{-3} Nm^{-1}), ρ is the liquid (precursor solution) density (10^{-3} kg m^{-3}) and f is the ultrasound frequency (10^{-6} s^{-1}).

The predicted particle size, D_p, can be expressed as a function of the droplet size, D_0, in accordance with the following relation [17]:

$$D_p = \left(\frac{M_{oxide}}{M_{prec.}}\frac{c}{\rho}\right)^{0.33} D_0 \quad (2)$$

where D_p is the particle mean size (μm), c is the mass concentration of the precursor solution (10^{-3} kg m^{-3}), M_{oxide} is the molecular mass of the resulting compound (g mol^{-1}) and $M_{prec.}$ is the molecular mass of precursor salt (g mol^{-1}).

The values estimated were as follows: $D_0 = 2.74$ μm and $D_p = 0.37$ μm (375 nm).

After synthesis, the powders were isothermally annealed in air at 800–1300 °C for 12 h (chamber furnace CHESA) to promote phase crystallization.

The physicochemical properties of the precursor solutions were carefully controlled and monitored as follows: pH 2.56 (Orion Research pH/millivoltmeter 611); density, $\rho = 1.01493 \times 10^{-3}$ kg m^{-3} (AP-PAAR density meter DMA 55), surface tension, $\sigma = 64.4 \times 10^{-3}$ Nm^{-1} (Digital K10T Kruss tensiometer) and viscosity, $\nu = 1.064315758 \times 10^{-3}$ Pa s (MLW Viscosimeter B3). Measurements were made at room temperature.

2.2. Particle characterization

The crystal structure of the ''*as-prepared*'' and thermally treated powders was analyzed by X-ray diffraction (XRD) in

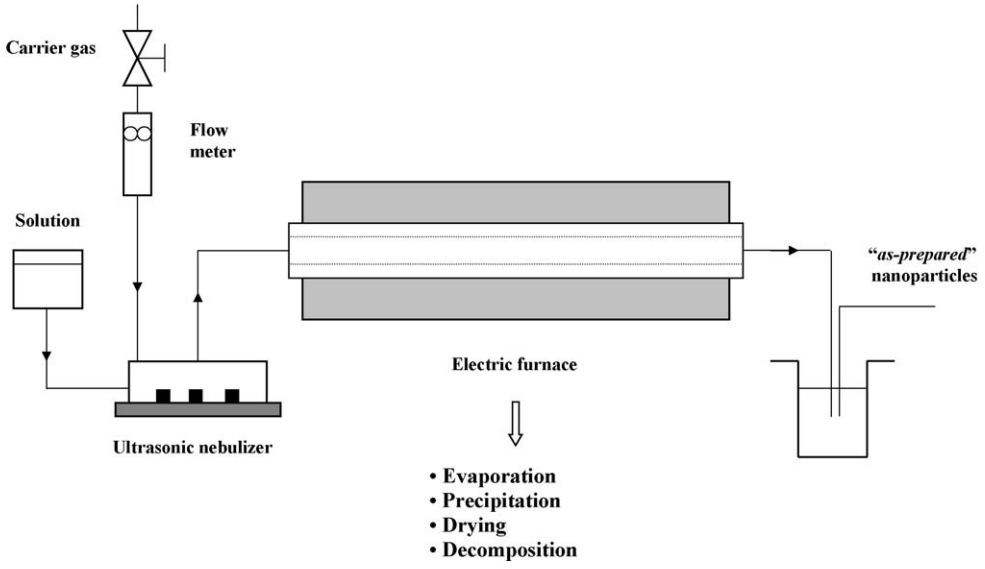

Fig. 1. Schematic representation of the processing equipment.

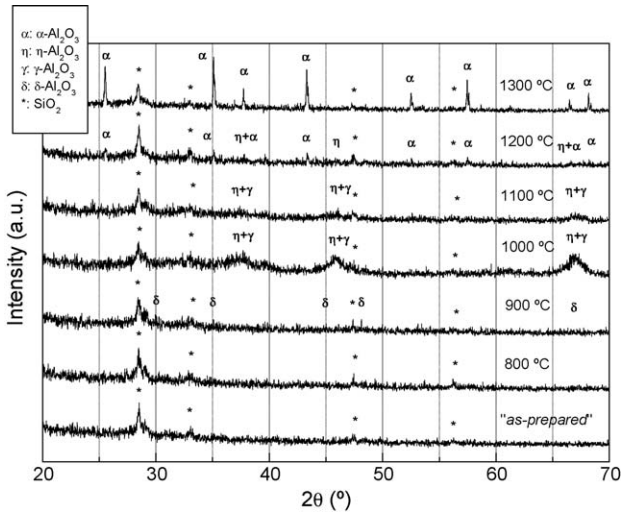

Fig. 2. Experimental X-ray diffraction patterns for "*as-prepared*" and thermally treated powder samples.

combination with electron diffraction–HRTEM. An automatic X' Pert Philips diffractometer, using a CuKα source (λ = 1.5418 Å), in the 20–70° 2θ range in the step-scanning mode with a step size of 0.04° was used. Crystalline phases were identified and indexed by means of X-ray Diffraction Philips Analytical [18] software and the Pcpdfwin database – JCPDS-ICDD [19]. Electron diffraction and HRTEM were interpreted using Electron Diffraction Pattern Simulations for Windows and Digital Micrograph programs [20].

Chemical composition, homogeneity and particle morphology were examined by scanning electron microscopy (SEM)

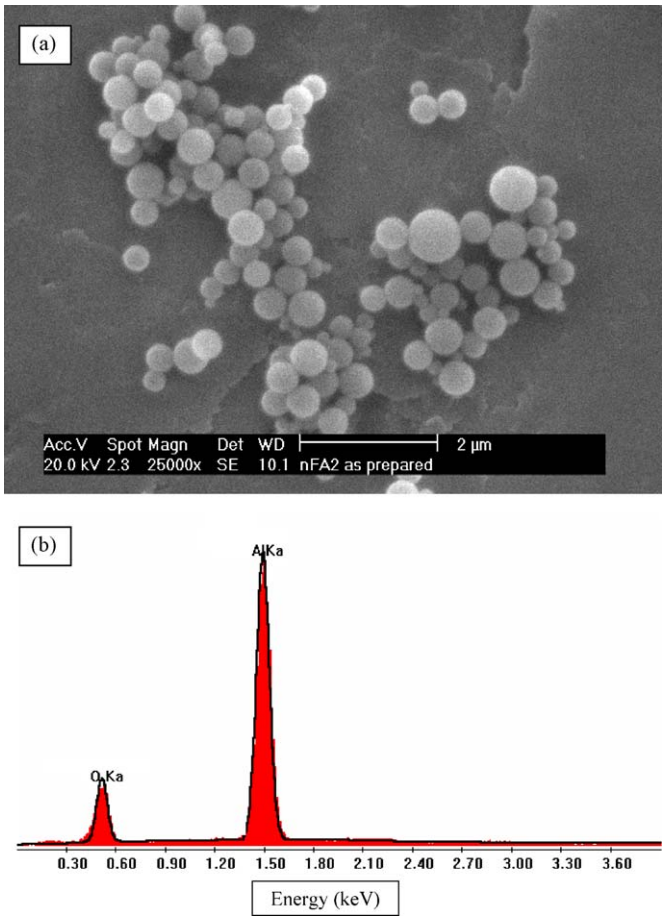

Fig. 3. (a) SEM micrograph of "*as-prepared*" Al_2O_3 particles and (b) corresponding EDS analysis.

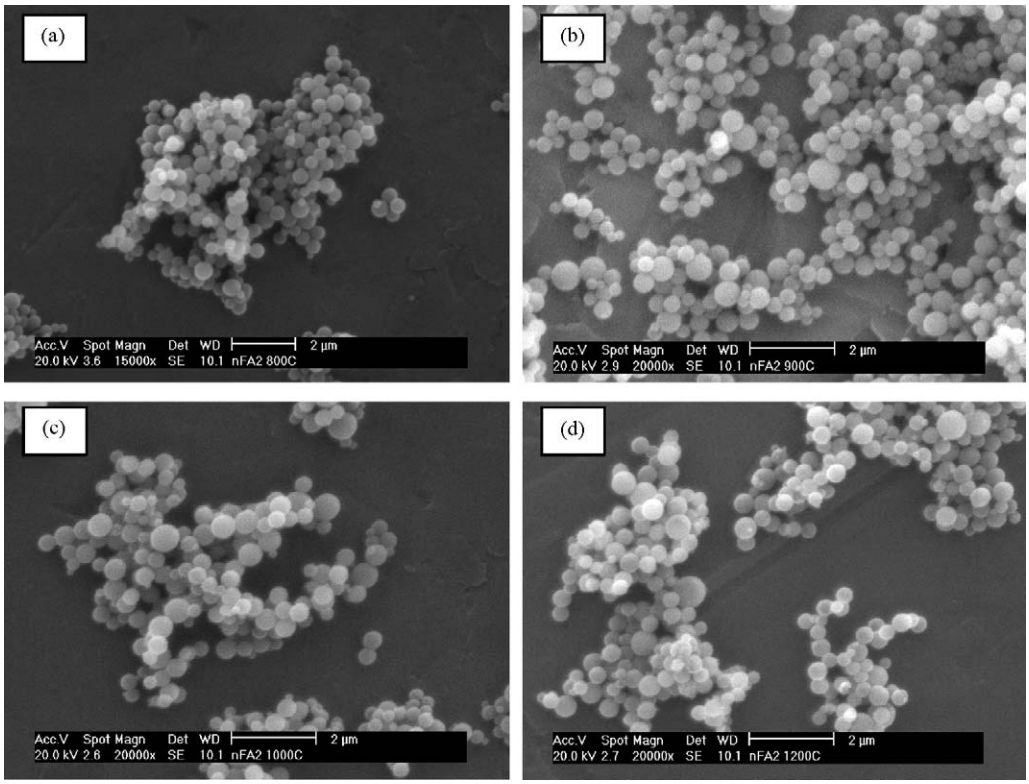

Fig. 4. SEM micrographs of the thermally treated powder samples: (a) 800 °C/12 h, (b) 900 °C/12 h, (c) 1000 °C/12 h and (d) 1200 °C/12 h.

equipped with energy dispersive X-ray analysis (EDAX) on a Philips XL 30 and transmission electron microscopy (TEM, JEOL-JEM, 400 kV). Prior to SEM analysis, the particles were ultrasonically disagglomerated for 10 min in an ultrasonic bath, disposed onto aluminium substrate and sputtered with gold. TEM samples were prepared by ultrasonic dispersion of a small portion of powder in acetone; this suspension was further placed on a 3-mm carbon coated copper grid.

Primary nanoparticles were identified using the JEOL JEM 4000EX, operated at 400 kV with a resolution of 1.8 Å (point to point). Digital images were processed using digital Micrograph™ software package. Measurements were carried out using pixel scale (1 pixel: 0.625 nm × 0.625 nm, in this case 1 nm = 1.6 pixels). Primary particles were identified as individual particles with different contrasts and visually perceptible contour features. Measurements of the D_{max} were carried out manually.

3. Results and discussion

Fig. 2 shows the XRD results obtained for the "*as-prepared*" (700 °C) and thermally treated powder samples. In the "*as-prepared*" as in samples after a thermal treatment at 800 °C the amorphous character is typically reflected in the shape of the patterns. Only after a thermal treatment at 900 °C some evidences of the presence of the δ-Al_2O_3 phase (JCPDS = 16-0394, a = 7.943 Å, c = 23.5 Å) are identified as low intensity reflections. With a thermal treatment at 1000 °C the η-Al_2O_3 phase (JCPDS = 04-0875) and the beginning of the cubic γ-Al_2O_3 phase (JCPDS = 10-0425, Fd3m, SG 227, a = 7.9 Å) with well-defined peaks at 1.94 Å ($2\theta = 45^\circ$), 1.39 Å ($2\theta = 67^\circ$) and 2.39 Å ($2\theta = 37.61^\circ$) are identified, and prevail after the thermal treatment at 1100 °C. The η-Al_2O_3 phase continues after the thermal treatment at 1200 °C and the α-Al_2O_3 phase (JCPDS = 10-0173, R−3c, SG 167, a = 4.758 Å, c = 12.99 Å) begins to appear with peaks at 2.08 Å ($2\theta = 43.3^\circ$), 2.55 Å ($2\theta = 35.1^\circ$) and 1.6 Å ($2\theta = 57.51^\circ$). After the thermal treatment at 1300 °C/12 h only well-defined peaks of the α-Al_2O_3 phase are identified. Associated with these phases, in all the XRPD there is a contamination of SiO_2 from the quartz tube (marked as *). The polymorph of SiO_2 is irrelevant for the material obtained, because it represents a contamination made during powder collecting (some powder charges were scratched from the quartz tube during collecting), it appears only in one or two charges and it does not represent either the characteristic of the materials obtained or the process (aerosol synthesis). XRPD shows signals not consistent with the typical SiO_2, but with another phase of SiO_2 known as keatite (tetragonal form of silica, JCPDS = 76-0912, a = 7.46 Å, c = 8.61 Å) which can be present metastably in the presence of steam over a temperature range of 300–600 °C and a pressure range of 400–4000 bar.

After the diffraction maxims in all the samples including thermal treatments, the possibility to find the β-quartz would be the expected phase but the closest phase related is the Keatite. However there is not written enough about this phase and in many cases authors talk about solid solutions with keatite associated to glass-ceramic [21].

Fig. 3a shows scanning electron microscopy micrographs of the "*as-prepared*" Al_2O_3 particles. It can be observed that the "*as-prepared*" particles obtained by aerosol decomposition are spherical, smooth, non-aggregated and relatively uniform in size (≤400 nm). EDAX analyses (Fig. 3b) confirm high compositional uniformity and the exclusive presence of the constitutive elements (Al and O).

Fig. 4 corresponds to SEM images taken with secondary electron mode detector for thermally treated powder samples at 800–1200 °C during a 12 h period. It can be observed that the particle morphology does not change significantly with annealing. Powders persist in their unagglomerated form, although high temperature regime brings about further crystallization and the growth of primary particles [9]. Thermal treatment at 1300 °C/12 h results in significant change in particle morphology, which is illustrated in Fig. 5, showing non-spherical and aggregated particles. This thermal treatment provokes the bonding of particles and sintering, followed by the neck formation.

Low magnifications in bright field mode allowed identification of the primary nanoparticles which are presumably aroused through the collision/coalescence mechanisms [9]. Fig. 6 shows two low magnification TEM images in bright

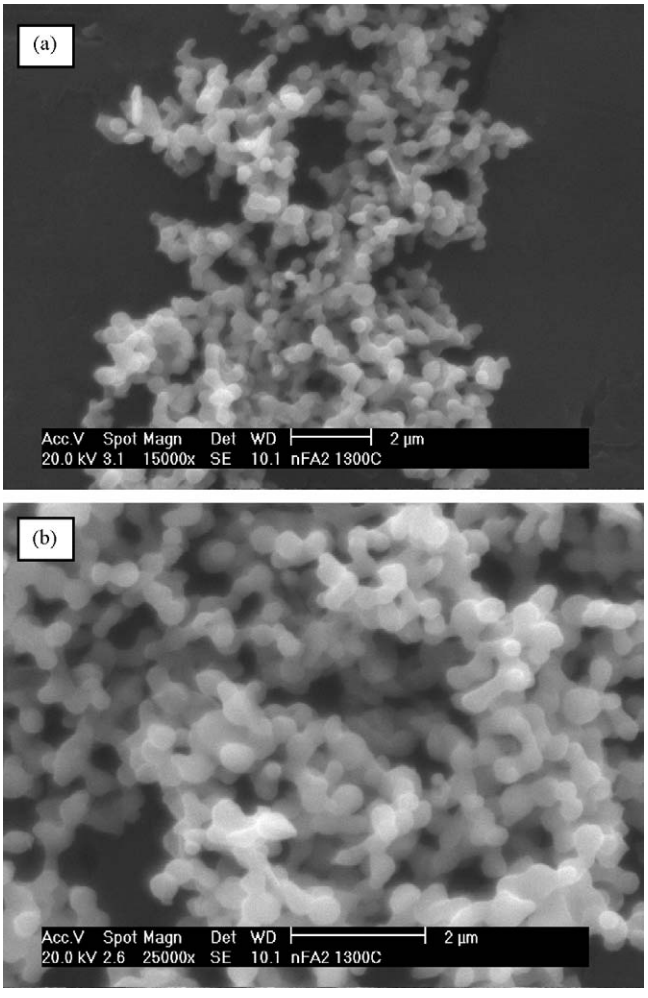

Fig. 5. SEM micrographs of sample annealed at 1300 °C/12 h.

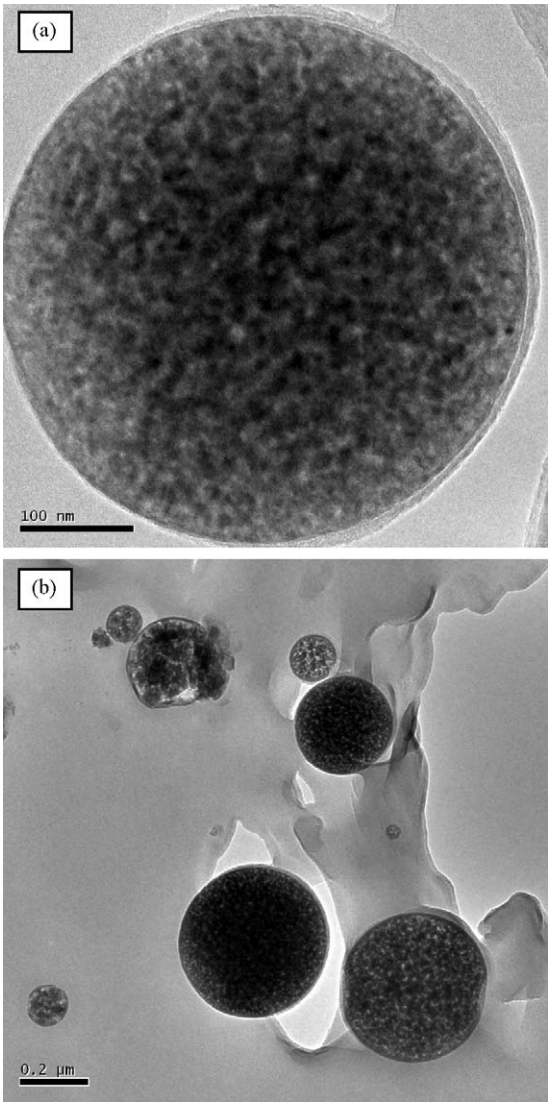

Fig. 6. Low resolution TEM images in bright field mode for Al_2O_3 after an isothermal treatment at 1100 °C/12 h.

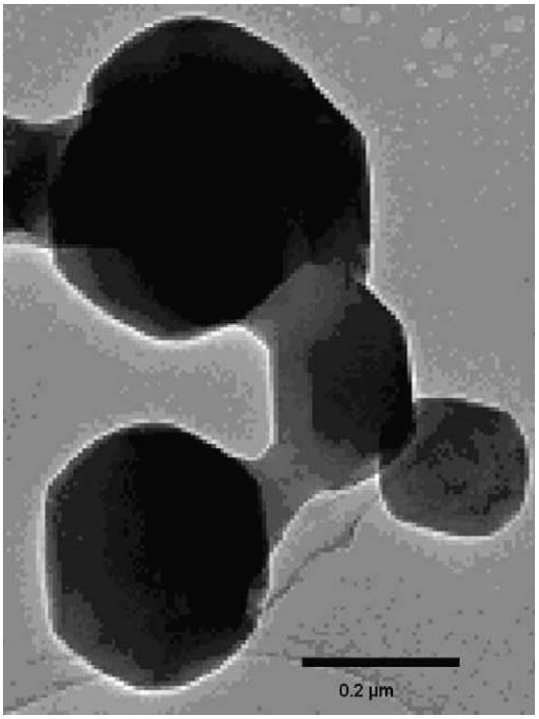

Fig. 7. Low resolution TEM image in bright field mode for Al_2O_3 after an isothermal treatment at 1300 °C/12 h.

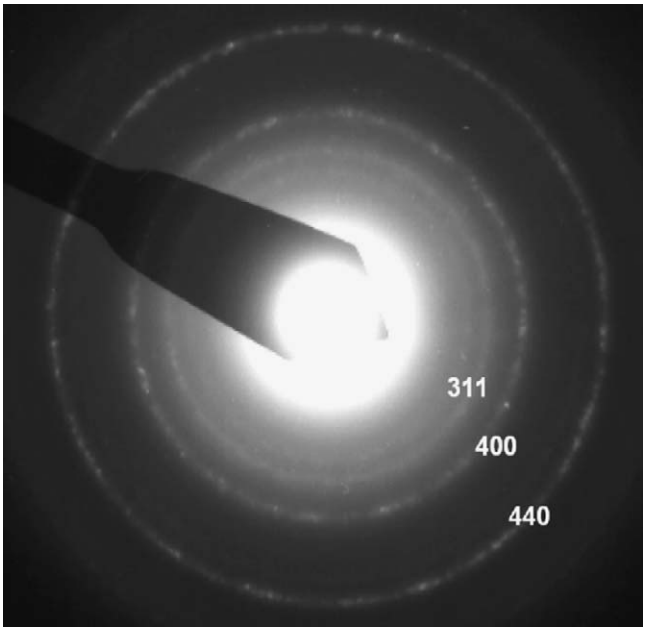

Fig. 8. SAEDP of the sample annealed at 1100 °C/12 h indexed according to the γ-Al_2O_3 phase.

field mode of secondary particles, annealed at 1100 °C/12 h. In Fig. 6a is observed an image of a secondary particle of 480 nm diameter. Further magnification and contrast analysis reveal small subspheric primary nanoparticles with $D_{max} = 13.5 \pm 4$ nm. The contrast at the external edge of the particles suggests the presence of approximately 8–11 nm thick crust at the particle surface. In Fig. 6b are observed images of secondary particles with different diameters (<425 nm). The amorphous and polycrystalline characters of the particles, typical for the ''*as-prepared*'' and thermally treated samples, did not allow the acquisition of high-quality HRTEM images. On the contrary, isothermal treatment at 1300 °C/12 h provokes the particle bonding and sintering, followed by neck formation, as evident in the low magnification TEM image (Fig. 7).

Fig. 8 shows a selected area electron diffraction pattern (SAEDP) taken from the sample annealed at 1100 °C/12 h indexed in accordance with the γ-Al_2O_3 phase (JCPDS = 29-0063), having a defect spinel structure [22,23]. Fig. 9 corresponds to the selected area electron diffraction pattern (SAEDP) obtained for the sample annealed at 1300 °C. The maximum is indexed based on a rhombohedral R−3c structure (167) typical of the α-Al_2O_3 phase similar to Martín, M.I. et al. [15].

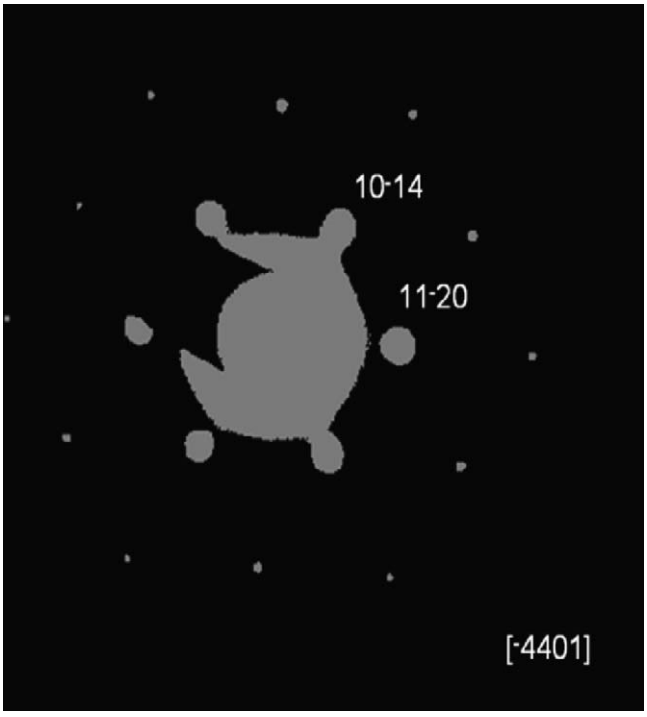

Fig. 9. SAEDP of the sample annealed at 1300 °C/12 h, along the [-4401] zone axis indexed according to the α-Al_2O_3 phase.

4. Conclusions

The paper presents the aerosol synthesis at 700 °C of fine Al_2O_3 particles (<400 nm) followed by X-ray powder diffraction (XRPD) and electron microscopy characterization (SEM and TEM). The "*as-prepared*" particles and samples treated at temperatures up to 800 °C are amorphous. XRPD and electron diffraction–HRTEM show the presence of two polycrystalline phases after the high temperature treatment: η and α, the latter prevailing at 1300 °C/12 h. Microscopic observations indicate that the obtained Al_2O_3 particles are spherical, smooth and non-agglomerated. High temperature (800–1200 °C) annealing did not have significant impact on the particle morphology. Owing to well-controlled and well-defined properties, these nanostructured particles could presumably be applied in discontinuous reinforcement for MMCs.

Acknowledgments

The authors gratefully appreciate the financial support of the Ministry for Education and Science of Spain, Juan de la Cierva Program JCI-2005-1892-13 (M.I. Martín), MAT2006-02458 project, Sabatic Grant SAB 2004-0035 and Project142010, Ministry of Science, Serbia (O. Milosevic). The assistance in TEM characterization of the Electron Microscopy and Citometry Center of University Complutense de Madrid (Spain) is also kindly acknowledged.

References

[1] P.A. Zieliński, R. Schulz, S. Kaliaguine, A. Van Neste, Structural transformations of alumina by high energy ball milling, J. Mater. Res. 8 (11) (1993) 2985–2992.
[2] L.L. Hench, Bioceramics: from concept to clinic, J. Am. Ceram. Soc. 74 (1991) 1487–1510.
[3] N. Travitzky, P. Kumar, K.H. Sandhage, R. Janssen, N. Claussen, Rapid synthesis of Al_2O_3 reinforced Fe–Cr–Ni composites, Mater. Sci. Eng. A 344 (1–2) (2003) 245–252.
[4] P. Ganguly, Poole, J. Warren, In situ measurement of reinforcement stress in an aluminium–alumina metal matrix composite under compressive loading, Mater. Sci. Eng. A 352 (1–2) (2003) 46–54.
[5] E. Martínez Flores, J. Negrete, G. Torres Villaseñor, Structure and properties of Zn–Al–Cu alloy reinforced with alumina particles, Mater. Des. 24 (3) (2003) 281–286.
[6] S.F. Hassan, M. Gupta, Development of high-performance magnesium nano-composites using solidification processing route, Mater. Sci. Technol. 20 (2004) 1383–1388.
[7] C.Y.H. Lim, S.C. Lim, M. Gupta, Wear behaviour of SiC_p–reinforced magnesium matrix composites, Wear 255 (2003) 226–229.
[8] Wang, Wei-Ning, Lenggoro, I. Wuled, Terashi, Yoshitake, Kim, Tae Oh and Okuyama, Kikuo, One-step synthesis of titanium oxide nanoparticles by spray pyrolysis of organic precursors, Mater. Sci. Eng. B 123 (3) (2005) 194–202.
[9] W. Koch, S.K. Friedlander, Particle growth by coalescence and agglomeration, J. Aerosol Sci. 21 (1) (1990) S73–S76.
[10] R. López Ibáñez, J.R. Ramos Barrado, F. Martín, F. Brucker, D. Leinen, Oxide barrier coatings on steel strip by spray pyrolysis, Surf. Coat. Technol. 188/189 (2004) 675–683.
[11] L. Castañeda, J.C. Alonso, A. Ortiz, E. Andrade, J.M. Saniger, J.G. Bañuelos, Spray pyrolysis deposition and characterization of titanium oxide thin films, Mater. Chem. Phys. 77 (3) (2003) 938–944.
[12] Takehisa Fukui, Satoshi Ohara, Makio Naito, et al., Performance and stability of SOFC anode fabricated from NIO–YSZ composite particle, J. Power Sources 110 (1) (2002) 91–95.
[13] M. Vallet-Regí, L.M. Rodríguez-Lorenzo, C.V. Ragel, A.J. Salinas, J.M. González-Calbet, Control of structural type and particle size in alumina synthesized by the spray pyrolysis method, Solid State Ionics 101–103 (1997) 197–203.
[14] M. Vallet-Regí, V. Ragel, J. Román, J.L. Martínez, M. Labeau, J.M. González-Calbet, Texture evolution of SnO_2 synthesized by pyrolysis of an aerosol, J. Mater. Res. 8 (1) (1993) 138–144.
[15] M.I. Martín, M.E. Rabanal, L.S. Gómez, J.M. Torralba, O. Milosevic, Microstructural and morphological analysis of nanostructured alumina particles synthesized allow temperature via aerosol route, J. Eur. Ceram. Soc. 28 (13) (2008) 2487–2494.
[16] R.L. Lang, Ultrasonic atomization of liquids, J. Acoust. Soc. Am. 34 (1) (1962) 6–8.
[17] T.-Q. Liu, O. Sakurai, N. Mizutani, M. Kato, J. Mater. Sci. 21 (10) (1986) 3698–3702.
[18] Software of Philips Analytical X-ray, Philips Electronics N.V., 1996–1999.
[19] Pcpdfwin program, version 1.1, September 1995.
[20] J.P. Morniroli, D. Vankieken, L. Winter, Electron Diffraction Pattern Simulations for Windows Program.
[21] Roos, Christian, Becker, Otmar, Siebers, Friedrich, Microstructure and stresses in a keatite solid-solution glass–ceramic, J. Mater. Sci. 42 (1) (2007) 50–58 (9).
[22] G. Paglia, Determination of the structure of γ-alumina using empirical and first principles calculations combined with supporting experiments, Doctoral thesis, Curtin University of Technology (February 2004).
[23] R.S. Zhou, R.L. Snyder, Structures and transformations mechanisms of the η, γ and θ transition aluminas, Acta Crystallogr. B 47 (1991) 617–630.